

Terahertz polarization conversion and sensing with double-layer chiral metasurface

Zi-Yang Zhang(张子扬), Fei Fan(范飞), Teng-Fei Li(李腾飞), Yun-Yun Ji(冀允允), Sheng-Jiang Chang(常胜江)

Citation: Chin. Phys. B . 2020, 29(7): 078707 . **doi:** 10.1088/1674-1056/ab9294
Journal homepage: http://cpb.iphy.ac.cn; http://iopscience.iop.org/cpb

What follows is a list of articles you may be interested in

Polarization conversion metasurface in terahertz region

Chen Zhou(周晨), Jiu-Sheng Li(李九生)

Chin. Phys. B . 2020, 29(7): 078706 . **doi:** 10.1088/1674-1056/ab9295

Broadband terahertz time-domain spectroscopy and fast FMCW imaging: Principle and applications

Yao-Chun Shen(沈耀春), Xing-Yu Yang(杨星宇), Zi-Jian Zhang(张子健)

Chin. Phys. B . 2020, 29(7): 078705 . **doi:** 10.1088/1674-1056/ab9296

High birefringence, low loss, and flattened dispersion photonic crystal fiber for terahertz application

Dou-Dou Wang(王豆豆), Chang-Long Mu(穆长龙), De-Peng Kong(孔德鹏), Chen-Yu Guo(郭晨瑜)

Chin. Phys. B . 2019, 28(11): 118701 . **doi:** 10.1088/1674-1056/ab44af

Terahertz coherent detection via two-color laser pulses of various frequency ratios

Xin-Yang Gu(顾新杨), Ke-Jia Wang(王可嘉), Zhen-Gang Yang(杨振刚), Jin-Song Liu(刘劲松)

Chin. Phys. B . 2019, 28(9): 098701 . **doi:** 10.1088/1674-1056/ab37fc

Theoretical investigation of tunable polarized broadband terahertz radiation from magnetized gas plasma

Xin-Yang Gu(顾新杨), Jin-Song Liu(刘劲松), Zhen-Gang Yang(杨振刚), Sheng-Lie Wang(汪盛烈), Ke-Jia Wang(王可嘉)

Chin. Phys. B . 2018, 27(5): 058701 . **doi:** 10.1088/1674-1056/27/5/058701

SPECIAL TOPIC — Terahertz physics

Terahertz polarization conversion and sensing with double-layer chiral metasurface*

Zi-Yang Zhang(张子扬)[1], Fei Fan(范飞)[1,†], Teng-Fei Li(李腾飞)[1], Yun-Yun Ji(冀允允)[1], and Sheng-Jiang Chang(常胜江)[2,‡]

[1] *Institute of Modern Optics, Nankai University, Tianjin* 300350, *China*
[2] *Tianjin Key Laboratory of Optoelectronic Sensor and Sensing Network Technology, Tianjin* 300350, *China*

(Received 21 March 2020; revised manuscript received 5 May 2020; accepted manuscript online 13 May 2020)

The terahertz (THz) resonance, chirality, and polarization conversion properties of a double-layer chiral metasurface have been experimentally investigated by THz time domain spectroscopy system and polarization detection method. The special symmetric geometry of each unit cell with its adjacent cells makes a strong chiral electromagnetic response in this metasurface, which leads to a strong polarization conversion effect. Moreover, compared with the traditional THz transmission resonance sensing for film thickness, the polarization sensing characterized by polarization elliptical angle (PEA) and polarization rotation angle (PRA) shows a better Q factor and figure of merit (FoM). The results show that the Q factors of the PEA and PRA reach 43.8 and 49.1 when the interval film is 20 μm, while the Q factor of THz resonance sensing is only 10.6. And these PEA and PRA can play a complementary role to obtain a double-parameter sensing method with a higher FoM, over 4 times than that of resonance sensing. This chiral metasurface and its polarization sensing method provide new ideas for the development of high-efficiency THz polarization manipulation, and open a window to the high sensitive sensing by using THz polarization spectroscopy.

Keywords: terahertz, chiral metasurface, polarization conversion, sensing

PACS: 87.50.U–, 78.67.Pt, 42.25.Ja, 07.07.Df **DOI:** 10.1088/1674-1056/ab9294

1. Introduction

The terahertz (THz) wave generally refers to the electromagnetic wave whose frequency is in the range of 0.1 THz to 10 THz between the microwave and infrared radiation. The THz technology has promising application potentials for its unique advantages, especially in the imaging,[1] sensing,[2] and communication.[3,4] The application of terahertz technology is inseparable from various functional devices. Among them, THz polarization optic devices, such as polarization converters and rotators are in urgent demand. Traditional polarization converters rely on the anisotropy of bulk materials to realize the phase retardation and polarization control.[5] However, most of materials in nature are lack of notable birefringence or optical activity in the THz regime, so the artificial metasurfaces have been paid much attention in THz polarization devices.[6–8]

Metasurfaces are artificial electromagnetic structures consisting of orderly arranged plane elements, which can manipulate amplitude, phase, and polarization of waves in space and time domain.[9–11] When the cell structure of metasurface has geometric chirality, it will have chirality for electromagnetic waves with the proper wavelength, which is similar to the medium composed of chiral molecules.[12] Chiral metasurface can break the mirror symmetry, realize polarization conversion and asymmetric one-way transmission.[13] The macroscopic physical phenomenon of chiral medium is optical activity (OA),[14] where there are the different propagation constants for the two orthogonal chiral photonic states: left circularly polarized (LCP) light and right circularly polarized (RCP) light.[15] The difference in propagation speeds and absorptions of LCP and RCP makes polarization rotation and circular dichroism, respectively, which lead to the polarization conversion and selection.[16] By designing the proper structures and symmetry, the metasurface can obtain strong electromagnetic chirality and achieve efficient polarization conversion.

In recent years, the chiral metasurfaces in the THz band have received extensive attention. Liu *et al.*[17] designed a single-layer chiral metasurface can realize broadband polarization conversion in THz region, the polarization conversion rate can reach 90%, but the transmittance is very low. Cheng *et al.*[18] demonstrated a chiral metasurface structure based on bilayer wire-split-ring resonators, realized linear-to-circular and linear-to-linear polarization conversion for THz waves, with

*Project supported by the National Key Research and Development Program of China (Grant No. 2017YFA0701000), the National Natural Science Foundation of China (Grant Nos. 61971242, 61831012, and 61671491), the Natural Science Foundation of Tianjin City, China (Grant No. 19JCYBJC16600), and the Young Elite Scientists Sponsorship Program by Tianjin, China (Grant No. TJSQNTJ-2017-12).

†Corresponding author. E-mail: fanfei@nankai.edu.cn
‡Corresponding author. E-mail: sjchang@nankai.edu.cn

© 2020 Chinese Physical Society and IOP Publishing Ltd

the polarization conversion rate exceeding 90%. In addition, Decker *et al.*[19] proposed a stacked and twisted split-ring resonators arranged in a $C4$ symmetric lattice, the eigenmodes are truly chiral and exhibits huge optical activity with a polarization rotation angle of 30°.

Metasurface also exhibits a strong localized resonance and enhancement on the fields, which can significantly improve the performance in sensing technology.[20–22] In recent years, many metasurfaces with different structures were proposed for THz sensors.[23–25] However, the present sensing mechanism is mainly based on its localized resonance effect of metasurface, and relies on monitoring the frequency shift of the resonance peak in the THz spectra caused by the changes of detected physical parameter. If we can utilize polarization conversion and selection effects of chiral metasurface, we can detect polarization parameters rather than the changes of the intensity spectrum for THz sensing, which may bring more information, higher sensitivity, and new physical perspective. However, the works related to THz sensing based on the polarization conversion of the chiral metasurface have rarely been reported yet.

In this paper, a double-layer chiral metasurface is demonstrated for THz polarization conversion and sensing. The THz resonance, chirality, and polarization conversion properties of a double-layer chiral metasurface have been experimentally investigated by THz time domain spectroscopy (THz-TDS) system and polarization detection method. The special symmetric geometry of each unit cell with its adjacent cells makes a strong chiral electromagnetic response in this metasurface, which leads to a strong polarization conversion effect. Moreover, compared with the traditional THz transmission resonance sensing for film thickness, the polarization sensing shows a better quality (Q) factor and figure of merit (FoM). This chiral metasurface and its polarization sensing method provide new ideas for the development of high-efficiency THz polarization conversion and high sensitive sensing.

2. Sample preparation

Our proposed chiral metasurface consists of two layers of metallic subwavelength structures and one layer of polyvinyl alcohol (PVA) film sandwiched in the middle, as shown in Fig. 1(a). Two metallic layers have the same structures with the special inversion symmetry along z axis, and the PVA film is used for the interval. The metallic metasurface structures with asymmetric double spiral ring pattern are fabricated by conventional photolithography and lift-off. The substrate is the BF33 glass with 500-μm thickness, and the metal structure with a thickness of 200 nm is periodically attached to the surface. Its structure parameters are shown in Fig. 1(c), where $l = 150$ μm, $h = 80$ μm, linewidth $w = 10$ μm, the lattice period $a = 200$ μm in the x-axis direction, and $b = 100$ μm in the y-axis direction. Figures 1(d) and 1(e) are the micrographs of single layer and double-layer metasurface, respectively.

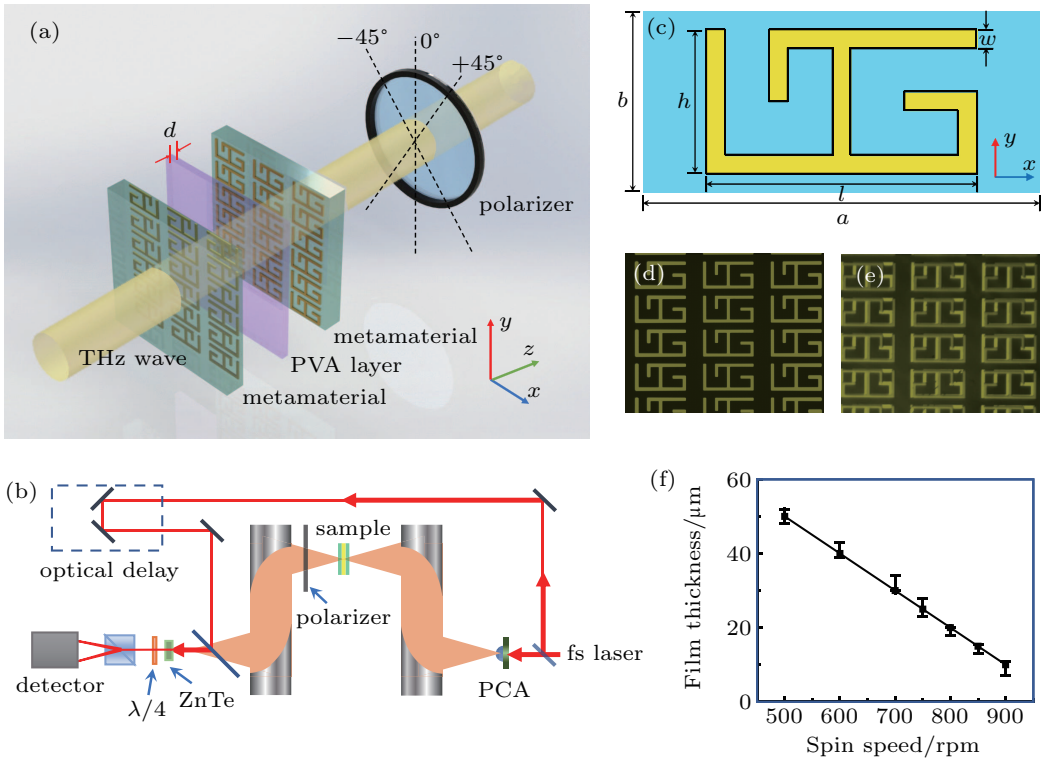


Fig. 1. (a) Schematic diagram of the proposed chiral metasurface and THz experimental configuration. (b) Schematic diagram of the THz-TDS system. (c) Geometry of the metasurface. Micrographs of the fabricated metasurface with (d) single layer and (e) double-layer. (f) Relationship between the spin speed and film thickness (the square points are the ideal film thickness, and the upper and lower horizontal short lines are the error ranges for multiple measurments).

The PVA is an important nontoxic and biocompatible polymer, and has a high transmittance in the THz regime. The PVA film is coated on one of the metallic metasurfaces. First, the PVA solution is prepared by mixing the PVA particles with de-ionized water, the weight ratio is 1 : 8. The mixture needs to be heated to 80 ℃ and magnetic stirred for hours until completely dissolved. Then the PVA film is processed by spin-coating the solution onto the metasurface. The thickness of PVA film can be controlled by adjusting the spin speed, so as to adjust the distance between two layers of metasurfaces, and the thickness is accurately measured by profilometer. Figure 1(f) shows the spin speed and film thickness are basically linear when the PVA solution's ratio is fixed, when the spin speed is increased from 500 rpm to 900 rpm, the thickness of the PVA film decreases from 50 μm to 10 μm.

The THz-TDS system is used in the experiments at room temperature with the humidity of less than 5% as shown in Fig. 1(b). The THz pulses are generated by a low-temperature grown GaAs photoconductive antenna excited by a Ti:sapphire femtosecond laser with 75-fs duration at 800 nm. A (110) ZnTe crystal is used for detection. The effective spectral range of this THz-TDS system is 0.05 THz to 2.5 THz, with a signal to noise ratio of 10^5 and 1.25-GHz resolution. THz waves are normally incident into the metasurface along z axis with a linearly polarized (LP) light along y axis. Unlike the standard THz-TDS system, a THz polarizer is placed behind the sample to detect the complete polarization state through the chiral metasurface. By rotating the direction of the polarizer, the THz time domain signal of the transmission wave in the directions of 0°, +45°, and −45° can be detected, as shown in Fig. 1(a).

3. Results and discussion

3.1. THz resonance property with linear polarization

Firstly, the transmission properties of the single-layer metasurface have been studied when the THz polarizer was rotated at 0°. When we rotate the metasurface at 0° and 90°, it is defined that the x-LP and y-LP incident transmissions of the metasurface are detected in the experiment, respectively. Figure 2(a) shows the experimental transmission spectra with different polarization states as well as the corresponding simulation results. The transmissions are determined by $T = |E_s(\omega)|/|E_r(\omega)|$, where $E_s(\omega)$ and $E_r(\omega)$ are the amplitude spectra of the sample and reference obtained by Fourier transform of the time domain pulses. The simulation results are calculated by the finite-difference time-domain (FDTD) method. The refractive index of glass substrate is set as 1.98, which is measured by experiment. The periodic boundary conditions are used in the x and y directions. When the electrical vector is parallel to the x direction, there is a 24-dB resonant dip at 0.704 THz, which is induced by the electric dipole resonance.[26] When the polarization direction is parallel to the y axis, there a 14-dB resonant dip will be excited at 0.785 THz. Therefore, the x-LP incidence is selected in all of the following experiments due to the larger resonance intensity.

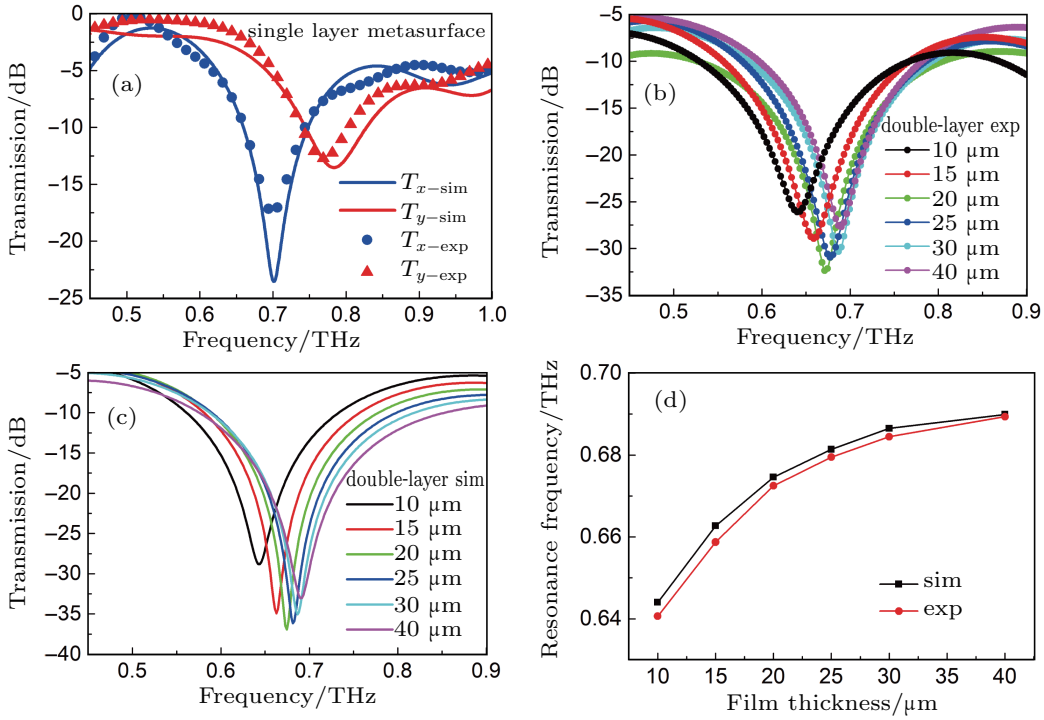


Fig. 2. (a) Experimental (exp) and simulation (sim) transmission spectra of the single-layer metasurface with x-LP and y-LP incidences, respectively. (b) Simulative and (c) experimental x-LP transmission spectra of double-layer chiral metasurface with different film thicknesses when the THz polarizer is rotated at 0°. (d) Relationship between the resonance frequency and the film thickness.

Next, we investigate the transmission spectra of the double layer chiral metasurface with x-LP incidence. Figures 2(b) and 2(c) show the experimental and simulative transmission spectra of the samples with different thicknesses of PVA film, respectively. The results show that the x-LP transmission spectra of double-layer metasurface are similar to that of single-layer structure, but the intensity of the resonance is always about 30 dB in both simulation and experimental results, which is much stronger than that of single-layer one shown in Fig. 2(a). As the thickness of the PVA film increases, *i.e.*, the interval between the two layers of metasurfaces increases, the blueshift of the resonant dip occurs. The results of experiment and simulation are in good agreement. The resonant frequency of the metasurface with 10-μm PVA film is located at 0.64 THz, while the resonant frequency moves to 0.69 THz when the PVA film increases to 40 μm. In this way, we can determine the thickness of thin film by measuring the resonant frequency of this metasurface through the THz-TDS system. The relationship between the film thickness and the resonance frequency is shown in Fig. 2(d), which is applied as a traditional THz sensing based on the resonance property of THz metasurface. In Subsection 3.3, we will compare the performance of this traditional sensing and new polarization sensing methods based on this chiral metasurface.

3.2. THz chirality and polarization conversion

To investigate the physical mechanism of the double-layer metasurface structure, the electric field distributions are simulated in Fig. 3. Figure 3(a) shows the electric field distribution in the front and back surface of the metasurfaces, which is rotating along the spiral structure of metasurface with time varying. In the same plane, the rotation direction of the two spiral structures is the same but rotated with 90°. This geometric rotation of 90° will cause an additional phase of 180° for the circularly polarized field, called as Pancharatnam–Berry phase.[27] Therefore, the rotation directions of the fields on the left and right spiral rings are the same but with a geometric phase of 180°. On the two corresponding front and back surfaces, the rotation directions of the fields are just opposite, and an additional geometric phase difference is −180°. Each cell has the mirror symmetry with its adjacent cells (*i.e.*, the left, right, front, and back). This configuration makes a strong chiral electromagnetic response. The front and back cell structures can be viewed as a coupled resonator system, where the strong chiral responses arise from the coupling in plane surface as well as up-lower surfaces, which can cause polarization conversion of THz waves. Figures 3(b)–3(d) show the distribution in the x–z plane with different PVA film thicknesses. The results show that the two metasurface E fields are coupled between front and back surfaces, and form a strong electromagnetic localized resonance in the PVA film. This enhanced resonant field has a distribution along the z direction, resulting in the shift of resonance frequency with the film thickness. As the thickness of the film increases, the influence on coupling is weakened, so that the frequency shift is not linear, but exponential attenuation with the increase of the PVA film thickness. When the thickness exceeds 40 μm, the electric field coupling between the two surfaces basically disappears, and the resonance frequency stops moving at 0.69 THz.

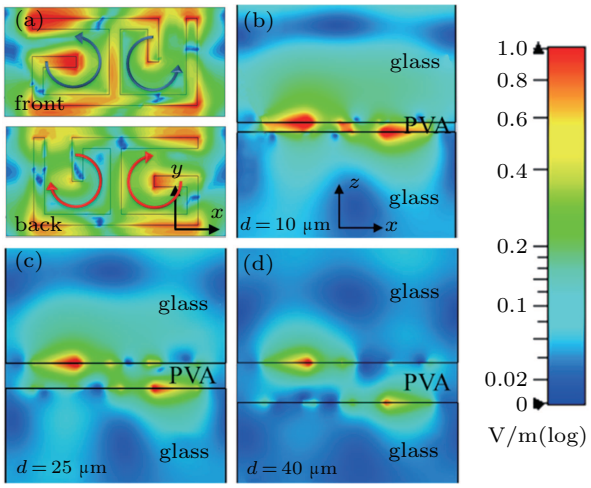


Fig. 3. (a) Electric field distribution in the x–y plane of the chial metasurface on the front and back surfaces with the film thickness $d = 10$ μm. The arrows indicate the direction of electric field rotating in the metasurface plane with the time varying. (b) Electric field distribution in the x–z plane, where the film thicknesses are 10 μm, (c) 25 μm, and (d) 40 μm, respectively.

To obtain the complete polarization state in the experiment, the THz polarizer behind the sample is rotated to detect the +45° and −45° LP components as shown in Fig. 1(a). In this method, we obtained the amplitudes and phases of two orthogonal linear polarization components of the output THz waves, so that the output polarization states in the broadband THz spectrum can be completely reconstructed. The THz-TDS signals of −45° and +45° LP components of chiral metasurface with the PVA film of 20 μm are shown in Fig. 4(a). After Fourier transform, frequency spectra can be obtained: the amplitude $A_{\pm 45^\circ}(\omega)$ and phase spectra $\sigma_{\pm 45^\circ}(\omega)$ for the +45° and −45° LP components, respectively. The transmission spectra of LCP and RCP components can be calculated by

$$\begin{aligned} T_{\mathrm{LCP}}(\omega) &= \frac{1}{2}\big(A_{+45^\circ}(\omega)\,\mathrm{e}^{\mathrm{i}\sigma_{+45^\circ}(\omega)} \\ &\quad - \mathrm{i}A_{-45^\circ}(\omega)\,\mathrm{e}^{\mathrm{i}\sigma_{-45^\circ}(\omega)}\big), \\ T_{\mathrm{RCP}}(\omega) &= \frac{1}{2}\big(A_{+45^\circ}(\omega)\,\mathrm{e}^{\mathrm{i}\sigma_{+45^\circ}(\omega)} \\ &\quad + \mathrm{i}A_{-45^\circ}(\omega)\,\mathrm{e}^{\mathrm{i}\sigma_{-45^\circ}(\omega)}\big). \end{aligned} \tag{1}$$

The corresponding transmission spectra of LCP and RCP are shown in Fig. 4(b). From the results, it can be seen that there is a large difference in the transmittance of LCP and RCP around 0.65 THz to 0.70 THz. There is a strong resonance at 0.66 THz

for the RCP wave, but a weak resonance at 0.7 THz for the LCP wave, which means there is a strong circular dichroism and polarization conversion within this frequency range.

Furthermore, the amplitude and phase of two orthogonal LP signals were processed to obtain two important polarization parameters, *i.e.*, the polarization elliptical angle (PEA) ε and polarization rotation angle (PRA) ψ, which can be derived as follows:

$$\tan 2\varepsilon = \sin 2\beta \sin \Delta\delta, \tag{2}$$

$$\tan 2\psi = \tan 2\beta \cos \Delta\delta, \tag{3}$$

where $\tan\beta = T_{+45^\circ}/T_{-45^\circ}$, $\Delta\delta = \sigma_{+45^\circ} - \sigma_{+45^\circ}$. The signs of PEA reflects the chirality of the output light, that positive values mean right-handed rotation and the negative values mean left-handed rotation. The PEA ranges from -45° to 45°, where 0° corresponded to LP wave, 45° corresponds to LCP wave and -45° corresponds to RCP wave. In fact, the spectrum of PEA is equivalent to the circular dichroism spectrum. The PRA ranges from -90° to 90°, where the polarization direction of the output wave was rotated with respect to the polarization direction of the incident wave. The clockwise direction of the PRA was positive, while the counterclockwise direction was negative.

The PEA and PRA spectra both in simulation and experiment are shown in Fig. 5. The simulation results are basically consistent with the experiment. It can be seen that both PEA and PRA have strong dispersions and special spectral lines, and reach the peak near the transmission resonance peak shown in Figs. 2(b) and 2(c). Both the PEA and PRA peaks have also a blue shift as the increase of the PVA film. For the experimental results shown in Figs. 5(c) and 5(d), all the PEA peaks are over 40°, the 20-μm and 25-μm cases reach 45°, which indicates the output waves are close to a good LCP state at the frequency of the PEA peak. The device realizes a highly efficient polarization conversion from LP light to LCP light. All the PRA peaks reach over 45°, and the polarization direction can rotate to 62° at 0.675 THz when the film thickness is 20 μm.

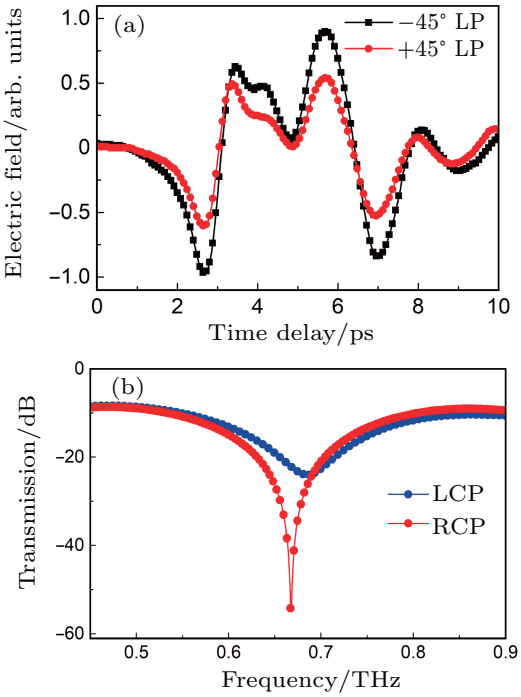


Fig. 4. (a) The THz-TDS signals of -45° and $+45^\circ$ polarization components for *x*-LP incidence when the thickness of the PVA film is 20 μm. (b) The corresponding transmission experimental spectra of LCP and RCP components of double-layer chiral metasurface.

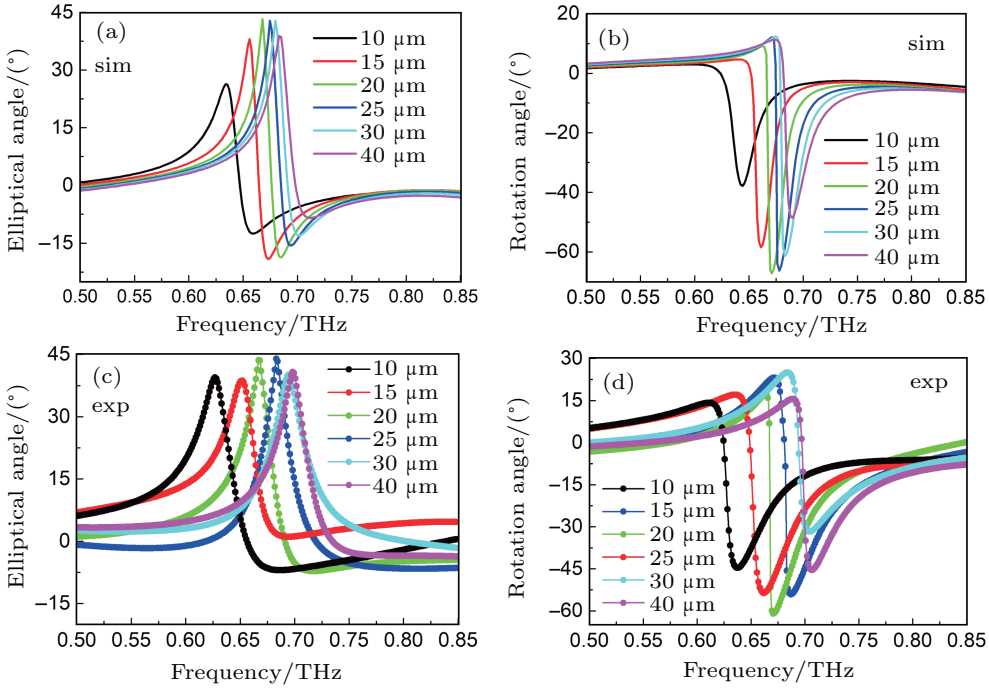


Fig. 5. Simulative (a) PEA and (b) PRA spectra, experimental (c) PEA and (d) PRA spectra of the double-layer chiral metasurface with different film thicknesses.

The terminal trajectory equation of electric vector E, also called as polarization ellipse, can be obtained as follows:

$$\left(\frac{E_x}{A_{-45^\circ}}\right)^2+\left(\frac{E_y}{A_{+45^\circ}}\right)^2-\frac{2E_xE_y}{A_{-45^\circ}A_{+45^\circ}}\cos\Delta\delta=\sin^2\Delta\delta. \quad (4)$$

Figures 6(a) and 6(b) show the polarization ellipses with different film thicknesses at 0.675 THz and 0.7 THz, respectively. At 0.675 THz, the polarization state changes from a right-handed oblate ellipse with -15° to the x axis to a good LCP state, and then continues to turn into a left-handed elliptical state with a positive angle to the x axis. In this process, the PEA of the output light changes dramatically. At 0.7 THz, the polarization state of the output light basically keeps LP state, but gradually rotates from 0° to -45°, that is the PRA changes a lot. Therefore, this chiral metasurface has a strong polarization conversion effect and changes dramatically with the interval thickness and frequency.

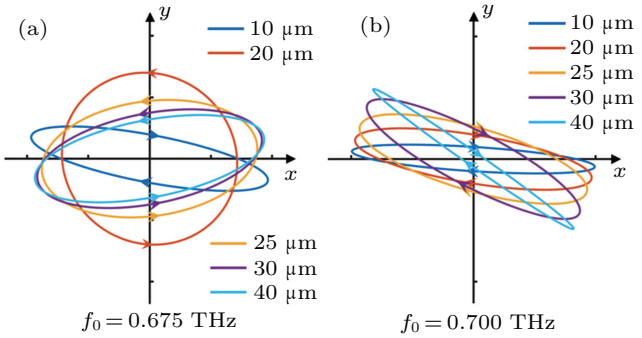


Fig. 6. Polarization ellipses of the output THz wave for x-LP incidence through the chiral metasurface with different film thicknesses at (a) 0.675 THz and (b) 0.7 THz.

3.3. THz polarization sensing

Finally, we discuss the THz polarization sensing performance based on this double-layer chiral metasurface compared with the traditional THz resonance sensing method. Three physical sensing parameters are considered: LP transmission resonance (TR) peak shown in Fig. 2 for the traditional THz resonance sensing, PEA peak and PRA peak shown in Fig. 5 for the new THz polarization sensing. Three evaluation indexes are defined to show the sensing performance, that is quality factor (Q), sensitivity (S), and FoM:

$$Q = f_0/\mathrm{FWHM}, \quad (5)$$

$$S = \Delta f/\Delta d, \quad (6)$$

$$\mathrm{FoM} = S/\mathrm{FWHM} = S\cdot Q/f_0, \quad (7)$$

where f_0 is the center frequency of spectral peak, FWHM is the full width at half maximum of the spectral peak, Δf is the frequency shift of the spectral peak, Δd is the corresponding change of film thickness.

Figure 7 shows these sensing evaluation indexes varying with the film thickness for the different sensing parameters TR, PEA, and PRA. The variation range and trend of center frequency are basically the same. The frequency shift ranges of PEA and PRA are slightly larger than that of TR as shown in Fig. 7(a), and the sensitivities for these three sensing parameters are nearly the same as shown in Fig. 7(c). The sensitivity decreases with the increase of the interval film from over 5 GHz/μm to lower than 0.5 GHz/μm. The sensitivities for the three different sensing parameters drop down when the film thickness is larger than 25 μm, because the electric field coupling of the two-layer metal metasurfaces weaken with the increase of the film thickness, as shown in Figs. 3(b)–3(d), the frequency shift is exponential attenuation with the increase of the film thickness. But the Q factors of PEA and PRA are much larger than that of TR as shown in Fig. 7(b). The Q factor reflects the sensitivity of the sensor itself, and is no relationship with the performance of the measuring system and the type of sample being tested. The Q factors of the PEA and PRA reache 43.8 and 49.1 when $d = 20$ μm, while the Q factor of TR is only 10.6. Compared with the traditional resonance sensing, the Q factor of polarization sensing is 4–5 times higher than that of resonance sensing by using the same metasurface device but the different sensing method.

FoM indicates a comprehensive performance of the sensor, the detected sample and the measuring system. Figure 7(d) shows that the FoMs of PEA and PRA are also much larger than that of TR, especially when the film thickness is small. When $d = 20$ μm, the FoM of PRA is up to 133 mm^{-1}, but the FoM of TR is only 29.8 mm^{-1}, which has 4.4 times. With the increase of film thickness, although the FoMs of three sensing parameters all drop down, the FoM of TR is only 1.91 mm^{-1} when $d = 40$ μm, while that of PEA remains a relatively large value of 26.7 mm^{-1}. Therefore, it shows that a better FoM can be obtained by using THz polarization sensing, compared by using the traditional resonance sensing. The FoMs also drop down dramatically when the film thickness is larger than 25 μm like sensitivity for the same reason. The different results are also obtained by using different polarization parameters. Here, when the film thickness $d < 25$ μm, the FoM of PRA is much larger than that of PEA, but when $d > 25$ μm, the FoM of PEA is larger than that of PRA. These two polarization parameters can play a complementary role in polarization sensing, therefore, this double-parameter sensing method is also better than the traditional single parameter sensing.

Furthermore, the sensing limitations of different sensing methods are discussed here. The sensing sensitivity of the sensor depends on the minimum frequency shift that the THz-TDS system can distinguish. However, the accuracy of the detected film thickness depends not only on the sensing measurement system, but also on the sensitivity of the sensor and the characteristics of the tested samples. According Eqs. (5)–(7),

the FoM can reflect the detection accuracy (A) of the sensing method, (*i.e.*, the minimum change of the film thickness that can be resolved) as $A = 1/\text{FoM}$. According to Fig. 7(d), the detection accuracy of three sensing methods can be obtained. Affected by the sensitivity of the sensor, the accuracy will decrease as the film thickness increases. The accuracies of the three sensing methods (TR, PEA, and PRA sensing) at 10 μm reach 13.7 μm, 5.9 μm, and 4.4 μm, respectively. It can be seen that the accuracy of THz polarization sensing is higher than that of resonance sensing.

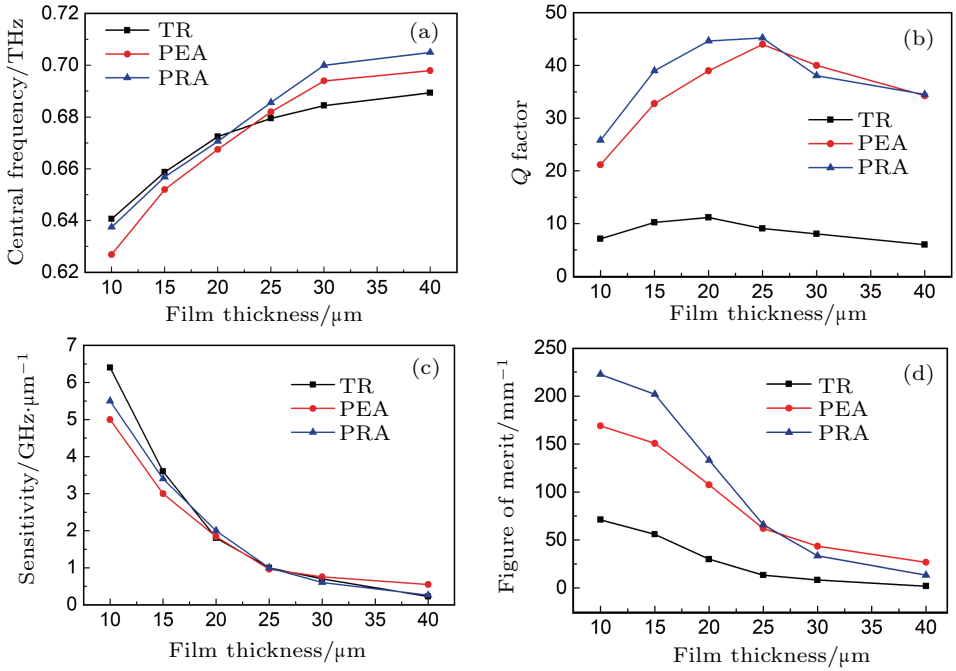


Fig. 7. Experimental evaluation indexes of sensing performance (a) central frequency, (b) Q factor, (c) sensitivity, and (d) FoM for LP transmission resonance peak, PEA peak, and PRA peak varying with the film thickness.

4. Conclusion

In conclusion, we have fabricated a double-layer chiral metasurface with a PVA film as interval between two layers of spiral metallic structures, and demonstrated that this metasurface can be applied in THz polarization conversion and sensing for film thickness by THz-TDS system and polarization detection method. The special symmetric geometry of each unit cell with its adjacent cells makes a strong chiral electromagnetic response in this metasurface, which leads to a strong polarization conversion effect. The chirality and polarization conversion performance of this chiral metasurface are characterized by PEA and PRA spectra. Moreover, compared with the traditional TR sensing, the polarization sensing characterized by PEA and PRA peaks shows a better Q factor and FoM, which is over 4 times than those of the TR sensing. And these PEA and PRA can play a complementary role in polarization sensing to obtain a double-parameter sensing method with a high FoM. This chiral metasurface and its polarization sensing method will provide new ideas for the development of high-efficiency THz polarization selection and manipulation, and open a window to the high sensitive sensing by using THz polarization spectroscopy.

Acknowledgment

The authors thank Prof. Peng-Fei Wu, Dr. Hong-Liang Liu and their research group from Institute of Modern Optics, Nankai University for providing the equipment of PVA film preparation.

References

[1] Jansen C, Wietzke S, Peters O, Scheller M, Vieweg N, Salhi M, Krumbholz N, Jördens C, Hochrein T and Koch M 2010 *Appl. Opt.* **49** E48
[2] Tu X C, Kang L L Xin H, Mao Q K, Wan C, Chen J, Jin B B, Ji Z M, Xu W W and Wu P H 2013 *Chin. Phys. B* **22** 040701
[3] Kleine-Ostmann T and Nagatsuma T 2011 *J. Infrared Millimeter Terahertz Waves* **32** 143
[4] Daryoosh Saeedkia 2013 *Handbook of terahertz technology for imaging, sensing and communications*, Vol. 1 (Woodhead Publishing) pp. 2, 3
[5] Kaveev A K, Kropotov G I, Tsygankova E V, Tzibizov I A, Ganichev S D, Danilov S N, Olbrich P, Zoth C, Kaveeva E G, Zhdanov A I, Ivanov A A, Deyanov R Z and Redlich B 2013 *Appl. Opt.* **52** B60
[6] Prinz V Y, Naumova E V, Golod S V, Seleznev V A, Bocharov A A and Kubarev V V 2017 *Sci. Rep.* **7** 43334
[7] Rahm M, Li J S and Padilla W J 2013 *J. Infrared Millimeter Terahertz Waves* **34** 1
[8] Mo W C, Wei X L, Wang K J, Li Y and Liu J S 2016 *Opt. Express* **24** 13621
[9] Monticone F and Alu A 2014 *Chin. Phys. B* **23** 047809
[10] Chen H Y, Wang J F, Ma H, Qu S B, Zhang J Q, Xu Z and Zhang A X 2015 *Chin. Phys. B* **24** 014201
[11] Smith D R, Pendry J B and Wiltshire M C K 2004 *Science* **305** 788
[12] Valev V K, Baumberg J J, Sibilia C and Thierry V 2013 *Adv. Mater.* **25** 2517

[13] Singh R, Plum E, Menzel C, Rockstuhl C, Azad A K, Cheville R A, Lederer F, Zhang W and Zheludev N I 2009 *Phys. Rev. B* **80** 153104
[14] Collins J T, Kuppe C, Hooper D C, Sibilia C, Centini M and Valev V K 2017 *Adv. Opt. Mater.* **5** 1700182
[15] Wegener M and Linden S 2009 *Physics* **2** 3
[16] Rodger A and Nordén B 1997 *Circular dichroism and linear dichroism*, Vol. 1 (Oxford: Oxford University Press) p. 2
[17] Liu W W, Chen S Q, Li Z C, Cheng H, Yu P, Li J X and Tian J G 2015 *Opt. Lett.* **40** 3185
[18] Cheng Z and Cheng Y 2019 *Opt. Commun.* **435** 178
[19] Decker M, Zhao R, Soukoulis C M, Linden S and Wegener M 2010 *Opt. Lett.* **35** 1593
[20] O'Hara J F, Withayachumnankul W and Al-Naib I 2012 *J. Infrared Millimeter Terahertz Waves* **33** 245
[21] Beruete Mand Jáuregui-López I 2019 *Adv. Opt. Mater.* **1900721**
[22] Cong L Q, Tan S Y, Yahiaoui R, Yan F P, Zhang W L and Singh R J 2015 *Appl. Phys. Lett.* **106** 031107
[23] O'Hara J F, Singh R, Brener I, Smirnova E, Han J G, Taylor A J and Zhang W L 2008 *Opt. Express* **16** 1786
[24] Chen M, Fan F, Shen S, Wang X H and Chang S J 2016 *Appl. Opt.* **55** 6471
[25] Neu J, Aschaffenburg D J, Williams M R C and Schmuttenmaer C A 2017 *IEEE Trans. Terahertz Sci. Technol.* **7** 755
[26] Aydin K and Ozbay E 2007 *J. Appl. Phys.* **101** 024911
[27] Berry M V 1984 *Proc. Roy. Soc. A: Math. Phys. Eng. Sci.* **392** 45